Inaccessible Pore Volume Formation During Sulfation of Calcined Limestones

Stratis V. Sotirchos and Solon Zarkanitis
Dept. of Chemical Engineering, University of Rochester, Rochester, NY 14627

A mathematical model for transport, reaction and structure evolution in gas-solid reactions with solid product is used to analyze a set of experimental data for the sulfation of calcines derived from three stones of high (>95%) calcium carbonate content. The analysis of the experimental data places emphasis on the formation of inaccessible pore space and its effects on the efficiency of calcined limestones as sorbents for SO_2 removal. Our results show that the ultimate capacity of calcined limestones for SO_2 uptake is influenced strongly by the formation of inaccessible pore space, which in turn is determined by their pore-size distribution and the connectivity (degree of interaction) of the pores. For the three specimens used in our study, the ultimate conversion (measured experimentally) increased and the inaccessible pore space formed during pore closure (predicted by the mathematical model) decreased with decreasing grain size in the rock precursors, indicating that the morphological texture of the precursors plays a major role in determining the topological features of the pore structure of the resulting calcines.

Introduction

During coal combustion, the sulfur contained in the coal matter is converted to sulfur oxides, primarily SO_2, which, if no action is taken, are emitted into the atmosphere with the flue gas. Sulfur dioxide emissions from coal-fired power plants account for the majority of the sulfur dioxide put into the atmosphere from man-made sources. Because of the role played by SO_2 in acid rain formation and the detrimental effects of acid rain on structures and terrestrial ecosystems, it is necessary that the sulfur content of the flue gas be reduced to an acceptable level before it is released into the atmosphere. In general, SO_2 emissions control can be achieved by intervening in the coal utilization process before, during or after combustion. Removal of sulfur dioxide during combustion is usually accomplished by feeding limestone or dolomite into the combustor in particle form. At the reaction conditions of the combustor, the carbonate particles decompose forming porous particles of the corresponding metal oxides, which react with the sulfur dioxide present in the reactor to form, depending on the reaction temperature, sulfates, sulfites, and sulfides or a mixture of these compounds (Chan et al., 1970).

A relatively large amount of theoretical and experimental work has been carried out on the investigation of the behavior of calcium oxide particles in an environment containing oxygen and sulfur dioxide. Most of the work has been done over the past two decades, a result of stricter environmental regulations on the operation of power plants. The experimental study of the reaction of SO_2 with porous CaO particles has mainly focused on studying the dependence of the overall rate of the reaction on the operating conditions and examining the relation of the reactivity and sorptive capacity of the porous sorbent to its physical properties. A number of interesting observations about the effects of particle size, calcination and sulfation temperature, and porosity and internal surface area (pore structure, in general) have been made in these studies (for example, Borgwardt, 1970; Hartman and Coughlin, 1974; Gullett and Bruce, 1987; Zarkanitis and Sotirchos, 1989). The conclusions reached by different investigators on the qualitative role played by the above factors and parameters in determining the reactivity and sorptive capacity of a sorbent are in relative agreement with each other, but there is much disagreement on their quantitative effects, especially for sorbents obtained from different limestone or dolomite precursors. A common general conclusion of almost all studies on the CaO-SO_2 reaction is that the physical properties of porous CaO-containing solids and, for particles derived from limestones and dolomites, of the parent rocks have the most influence in determining the efficiency of such solids as sorbents for SO_2

Correspondence concerning this article should be addressed to S. V. Sotirchos.

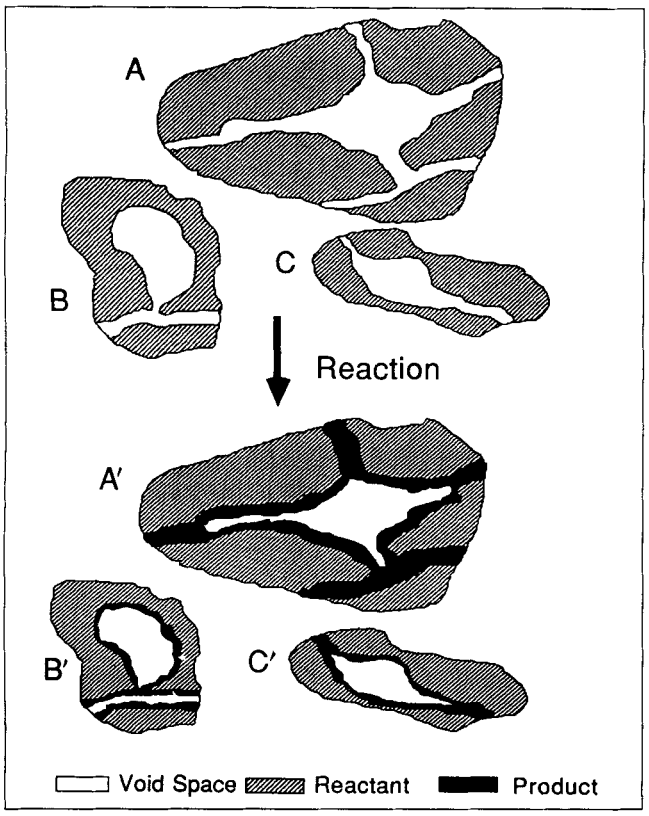

Figure 1. Inaccessible pore volume formation during a noncatalytic gas-solid reaction with solid product.

removal. Moreover, all studies agree that Ca:S ratios much larger than the stoichiometrically predicted 1:1 value must be used in practice for effective SO_2 removal.

The reaction of SO_2 with CaO or MgO is a gas-solid reaction with formation of a solid product, $CaSO_4$ or $MgSO_4$, that occupies more space than the solid reactant, CaO or MgO, from which it results. If no increase in the overall volume of the porous particles takes place during the reaction, the pore space may be completely filled with solid product. This takes place at about 50% conversion for porous CaO particles of 50% porosity. Once the pores become plugged with solid product, the interior of the porous particles is rendered practically inaccessible to the gaseous reactants inasmuch as diffusion through the solid product is an extremely slow process. If the reaction proceeds under significant diffusional limitations in the pore space, plugging of the pore openings may first occur at the external surface of the particles, leaving unusable open space in their interior and, therefore, lowering the ultimate (practically attainable) capacity of the sorbent for SO_2 removal to values below that predicted by the stoichiometry of the reaction for uniform filling of the particles with solid product. Plugging of the pores at the external surface with solid product is usually the main mechanism by which most of the mathematical models of the literature manage to reproduce experimental data for the CaO-SO_2 reaction. For a given particle size, the conversion profile in the interior of the particles depends on the relative rates of diffusion and reaction, which in turn are influenced strongly by the effective diffusivity in the pore space, its variation with the conversion, and the diffusivity in the product layer. It is thus these parameters that are used to fit predictions of the mathematical model to the experimental data. This approach is usually successful with experimental data obtained over relatively narrow ranges of operating conditions, but it fails to explain why solids of similar pore-size distributions may present substantially different capacities for SO_2 removal.

The structure of real porous media—as direct photomicrographic examination usually shows—consists of irregularly shaped pores, such as clusters of pores or cavities fed through smaller feeder pores (Figure 1A), ink-bottle pores (Figure 1B), and pores of varying cross-section along their length (Figure 1C). If the porous medium participates in a gas-solid reaction with solid product formation, the smaller pores (or more generally, the smaller openings) get plugged with solid product earlier forming inaccessible pore space as it is schematically shown in Figures 1A′, 1B′ and 1C′. Formation of inaccessible pore space limits the ultimate capacity of a porous sorbent (for example, of a calcined limestone for the problem studied in this study) for pollutant removal below the level that corresponds to complete pore plugging of the pore space with solid product even under conditions characterized by insignificant intraparticle diffusional limitations. Since the extent of formation of inaccessible pore space is influenced not only by the pore-size distribution of the solid but also by how the pores communicate with each other in the solid's interior, as the qualitative mechanisms portrayed in Figure 1 suggest, even solids with the same pore-size distribution can exhibit markedly different sorptive capacities.

A general mathematical model (generalized random pore model) was developed by Yu and Sotirchos (1987) for describing transport, reaction and structure evolution phenomena in gas-solid reactions with solid product formation. They built the model on the assumption that the pore structure of the solid can be represented by a network of pores of some size distribution, with the pore segments arranged around the bonds of a three-dimensional lattice. This model is thus capable of describing almost all phenomena encountered in gas-solid reactions with solid product, including that of the formation of inaccessible pore space. Preliminary analyses of experimental data for the CaO-SO_2 and ZnO-H_2S reactions (Zarkanitis and Sotirchos, 1989; Zarkanitis et al., 1990) have shown that the generalized random pore model is an efficient tool for analyzing data for such reactions. The generalized pore model is used in this study to analyze in detail reactivity evolution data, obtained in our laboratory, for the sulfation of particles of two high-purity limestones, some of which we presented and discussed in a past study (Zarkanitis and Sotirchos, 1989) and particles derived from calcitic single crystals (Iceland spar). Our analysis places emphasis on the formation of inaccessible pore space, and it is used to show that differing connectivity of the pores in the structure may be the main reason for which same size particles of similar pore-size distribution exhibit different capacities for SO_2 removal.

Materials, Reaction Conditions, and Experimental Procedures

Experimental results obtained for calcines derived from solids of high CaO content are analyzed in this study: a limestone of very high $CaCO_3$ content distributed by Greer Limestone

Table 1. Composition of the Calcined Samples

Mineral	Georgia Marble (wt. %)	Greer Limestone (wt. %)	Iceland Spar (wt. %)
CaO	94.16	97.34	98.97
MgO	2.57	0.81	0.3
SiO_2	2.62	1.5	0.01
Al_2O_3	0.14	0.18	0.01
Na_2O	0.01	0.01	0.18
K_2O	0.03	0.04	0.01
Fe_2O_3	0.06	0.08	0.58
MnO	0.01	0.01	0.01
TiO_2	0.03	0.04	0.01
P_2O_5	0.22	0.29	0.01
Total	99.85	100.3	100.1

Co. (Greer limestone), a calcitic marble (Tate White Aggregate) distributed by Georgia Marble Co. (Georgia marble), and a calcite in single crystal form distributed by Wards Inc. (Iceland spar). The chemical composition of the calcines of these solids was analyzed by X-ray fluorescence (X-Ray Assay Labs. Ltd.). The obtained results are shown in Table 1. The CaO content of the calcitic marble is slightly lower than that of the Greer limestone and of the Iceland spar (94.16% vs. 97.34% and 98.37%), but the former contains more MgO which might also react with SO_2.

Mercury porosimetry showed that the precursors (as received samples) were nearly nonporous. Further analysis of the rocks using gas adsorption revealed some small porosity (for pores smaller than 1,000 Å) which decreased in the direction Greer limestone → Georgia marble → Iceland spar (0.015, 0.007, and 0.004, respectively). Mineralogical analysis of the precursors found that the calcium carbonate was present in the form of calcite. Petrographic examination of the Greer limestone showed that it consisted of calcitic, microgranular mud with inclusions of aggregates of larger calcitic grains. The Georgia marble sample, on the other hand, was found to be spanned primarily by coarse calcitic grains. At the boundaries of the grains, small grains of iron oxide and quartz were observed to occur in both limestones. The Iceland spar sample was, of course, found to exist in the form of large single crystals.

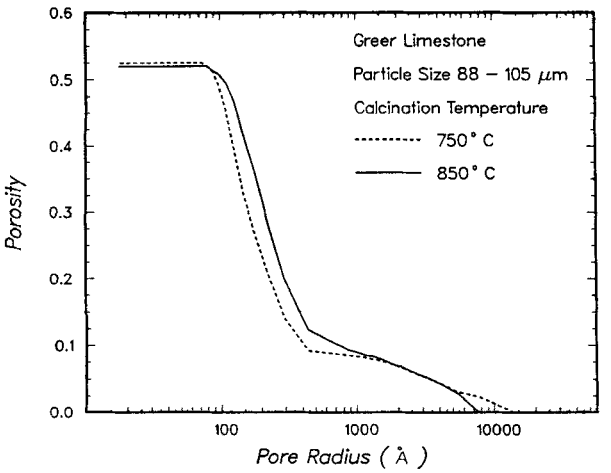

Figure 2. Pore-size distribution of Greer limestone calcines.

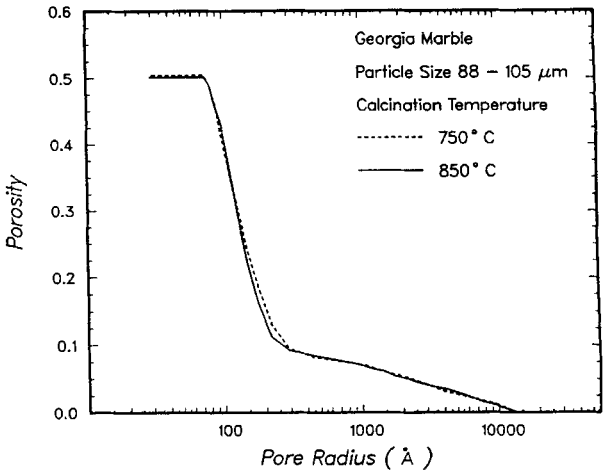

Figure 3. Pore-size distribution of Georgia marble calcines.

The three rocks were calcined, in particle form, under N_2 at 750 and 850°C. Sulfation experiments were conducted at 700, 750 and 850°C using a mixture of 3,000 ppm SO_2 and 12% O_2 in N_2, which was obtained by diluting a 0.5% mixture of SO_2 in air with N_2. All gases were at least of 99.99% purity and were supplied by Air Products Co. To differentiate the effects of structure evolution from those of intraparticle mass transport limitations, experiments were carried out using four particle size ranges: 53–62, 88–105, 210–250 and 297–350 μm. The particles were considered spherical in the analysis of the experimental data, and the arithmetic mean of the two limits of each size range was taken as average size. Reactivity experiments were carried out in a thermogravimetric analysis (TGA) system. The flow rate of the reactant mixture in the hangdown tube of the TGA system was kept at 250 mL/min in all experiments, and about 2–4 mg of uncalcined solid—the smaller amounts were used for the smaller particles—was employed in each experiment. A more detailed discussion of experimental procedures used during reactivity experiments can be found elsewhere (Zarkanitis and Sotirchos, 1989; Zarkanitis, 1991).

Mercury porosimetry and gas adsorption were used for pore structure characterization. Physical adsorption measurements for surface area determination were carried out in a flow-type reaction/adsorption apparatus (Crowley, 1985; Sotirchos et al., 1988) and in a volumetric system. The pore-size distributions of the produced calcines at the two calcination temperatures employed in our study are shown in Figure 2 for Greer limestone, Figure 3 for Georgia marble, and Figure 4 for Iceland spar samples. These pore-size distributions were obtained from the mercury porosimetry data by assuming a perfectly interconnected network of cylindrical pores. (A perfectly interconnected network of pores can loosely be defined as one in which all pores are infinitely long (that is, all pores reach the external surface) or one in which each pore segment is connected to at least one pore segment of larger size located closer to the external surface of the porous medium.) The BET method was employed for surface area estimation from gas adsorption (N_2 at 77 K) data (Gregg and Sing, 1982). The measured surface areas for various samples and calcination temperatures are given in Table 2. The relatively large amounts

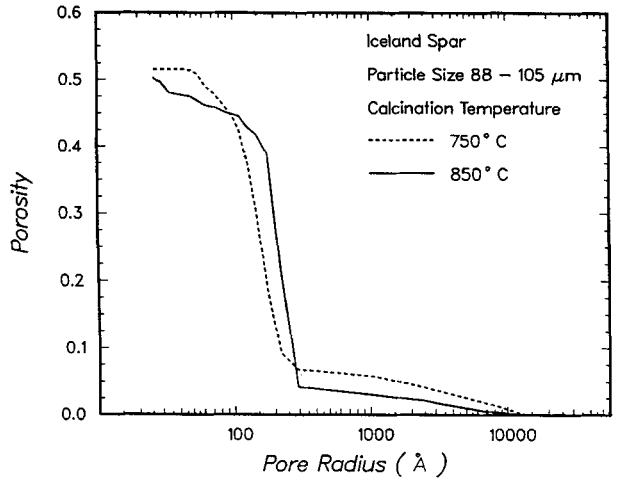

Figure 4. Pore-size distribution of Iceland spar calcines.

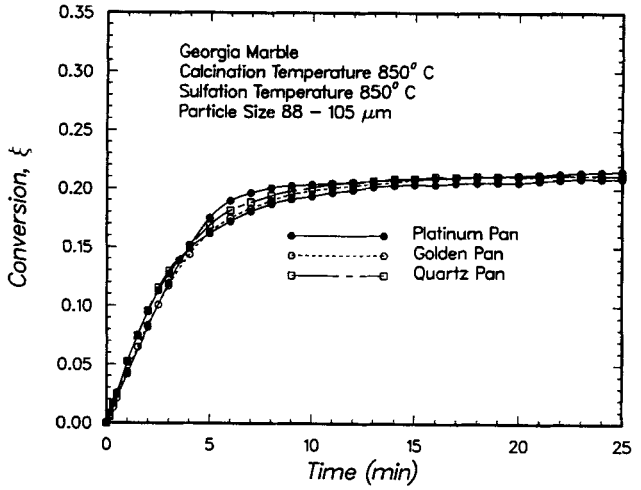

Figure 5. Effect of pan material on reactivity evolution curves.

of solid sample needed for pore structure characterization (about 250 mg) were prepared by calcination in a fixed-bed arrangement in small batches (*in situ* in the reaction/adsorption system) or a fluidized-bed reactor. Even though the flow rates used in the fixed-bed reactor were much smaller than those employed for fluidization, no significant pore structure differences were found to exist between samples prepared at the same temperature.

Table 2 shows that the surface area per unit mass of calcined sample decreased with increasing calcination temperature; Figures 2 and 4 show that part of the pore-size distributions of the Greer limestone and Iceland spar calcines was shifted toward larger pores. The calcination temperature (see Figure 3) appeared not to have any effect on the pore-size distribution of Georgia marble. The particle size did not influence significantly the surface areas of Greer limestone and Georgia marble, but it had (see Table 2) a more noticeable effect on the surface area of the Iceland spar calcines. Heat treatment under nitrogen at 850°C of the Georgia marble and Iceland spar calcines that were produced at 750°C decreased their surface area, probably because of sintering (see Table 2). Such behavior has been observed by several investigators (for example, Dogu, 1981; Borgwardt et al., 1986). The results shown and discussed in this study were obtained at sulfation temperatures lower than the calcination temperature to eliminate the possibility that structural changes caused by sintering could have taken place during the reaction. For the same calcination temperature, the surface area of the Georgia marble calcine was smaller than that of the Greer limestone sample, while Iceland spar had much higher surface area than other samples at all conditions studied. In contrast to the other two samples, the pore-size distribution of the Iceland spar calcines is of bimodal form, and it is probably the small pores that are responsible for its much higher surface areas. The pore structure characteristics of the six calcines will be discussed in more detail later in conjunction with the analysis of their reactivity data during sulfation.

In the high-temperature environment of the sulfation reactor, sulfur dioxide can react with oxygen to produce sulfur trioxide, which may in turn react with the metal oxide to give metal sulfates. Thermodynamic analysis of the oxidation of SO_2 indicates that a significant amount of SO_2 should be present as SO_3 at the conditions of our experiments (3,000 ppm SO_2, 1 atm, 12% O_2, and 700–850°C). Specifically, the equilibrium ratio of the partial pressure of SO_3 to that of SO_2 varies in the range [0.1, 1], decreasing with increasing temperature because of the exothermic nature of the reaction. However, the reaction rate is so slow that the produced amount of SO_3 is negligible even at the high end of the temperature range in the absence of a catalyst. Platinum, the material used for the hangdown wire and pan in the TGA, is one of the most efficient catalysts of the oxidation of SO_2 to SO_3 (Schroeter, 1966). To investigate the effects of possible sulfur dioxide oxidation on the measured reactivity evolution curves, test experiments were conducted using three pans made of gold, quartz, and platinum. Some of the obtained results are shown in Figure 5 for the Georgia marble sample calcined and sulfated at 850°C. The independence of the results of the pan material indicates that sulfur dioxide is the primary reactive species rather than sulfur trioxide. Even though sulfur trioxide is thermodynamically favored at lower temperatures, experiments at 700°C gave results similar to those of Figure 5. The catalytic effects of the platinum pan could have been diminished because of

Table 2. Surface Areas of the Calcined Samples (m^2/g)

Calcination Temp. (°C)	Georgia Marble (83–105 μm)	Greer Limestone (83–105 μm)	Iceland Spar (88–105 μm)	Iceland Spar (297–350 μm)
750	40.0	47.8	83.8	78.6
850	32.2	33.7	65.6	62.0
750*	38.4	47.4	64.1	57.0

*Followed by treatment under N_2 for 30 min at 850°C.

its extended use under sulfur dioxide and the short residence time of the reactive mixture in the neighborhood of the pan. Note that the results of Figure 5 could also be viewed as representative of the reproducibility and repeatability of our experimental data.

The use of 2-4 mg of sample and 250 mL/min flow rate in our experiments was the result of a detailed investigation of the effects of sample size on the thermogravimetric reactivity data (conversion vs. time curves). Large sample sizes slowed down the reaction considerably, especially during its initial stages where higher reaction rates prevailed. The sample size effects of the reactivity evolution curves were more pronounced for the small (53-62 μm) particles. Since these particles tended to agglomerate during the reaction, it was concluded that interparticle diffusional limitations were a contributing factor in the observed particle-size effects. Large samples sizes also led to nondifferential operation of the TGA reactor. For the reaction rates that are typically seen in CaO-SO_2 experiments, an overall mass balance on a gas-solid reactor shows that very high flow rates must be employed (over 2 L/min) to keep a reactor loaded with sample sizes larger than 50 mg operating in differential mode. Use of such flow rates is impossible in a TGA system since the flow rate in the hang-down tube must be kept below a certain limit for problem-free operation of the microbalance. We chose to work with flow rates of 250 mL/min because such rates were found to give an acceptable signal-to-noise ratio at temperatures as high as 900°C for the reactor tube configuration used in this study. Moreover, even for the highest reaction rates encountered in our experiments, a flow rate of 250 mL/min or above and 2-4 mg of calcine gave almost differential operation of the TGA reactor for the sample sizes used in our experiments. It should be pointed out that the above findings cast considerable doubt over most of the thermogravimetric reactivity data of the literature, especially for small reaction times, since in most cases both large sample sizes (over 100 mg in some cases) and low flow rates were employed.

Analysis of the Experimental Data

CaO and MgO contained in calcined limestones react with SO_2 in the presence of O_2 according to the overall reaction:

$$MO + SO_2 + \frac{1}{2} O_2 \rightarrow MSO_4;\ M = Ca \text{ or } Mg \qquad (R1)$$

At atmospheric pressure and in the presence of 12% (volume/volume) O_2 and 3,000 ppm SO_2, the reaction conditions used in our experiments, the sulfation of CaO is far from equilibrium at temperatures below 850°C, and consequently, it may be treated as an irreversible reaction. Although the solids used in our experiments contained very small amounts of MgO and inert solids, a rigorous treatment of the problem requires that some assumptions be made about the role played by these species in the reaction process. Thermodynamic analysis of the sulfation of MgO (Yu, 1987) shows that the reaction can take place under the conditions of our experiments since it reaches equilibrium at temperatures higher than 850°C, though not much higher. Working with reagent-grade MgO powder, we found (Zarkanitis, 1991) that at the conditions of our experiments, the sulfation of MgO proceeded at rates comparable to those of the sulfation of CaO. We will thus assume that CaO and MgO react at rates proportional to their concentrations in the unreacted solid phase so that a sharp reaction interface develops in the reacting solid particles. Various impurities are mixed homogeneously with the reactant species so that reaction occurs uniformly over the reaction interface.

In general, gas-solid reactions involving porous particles occur under conditions in which appreciable concentration gradients exist in the pore space. There are two gaseous reactants involved in the sulfation reactions: O_2 and SO_2, see Eq. R1. Since the concentration of oxygen is by more than an order of magnitude larger than that of sulfur dioxide, its profile in the intraparticle space will practically be uniform. The same will also be true for the temperature profile since because of the low concentrations of SO_2, small amounts of heat are released within the particles, which are not capable of raising the temperature significantly. The local mass balances of the gaseous and solid reactants (SO_2 and MO) in the interior of the particles, assumed to be spherical, are only needed to describe the diffusion and reaction problem in the intraparticle space. The resulting equations have the form:

$$\frac{\partial[\epsilon_p^a(\xi)c_p]}{\partial t} = \frac{1}{r^2}\frac{\partial}{\partial r}\left[r^2 D_e(\xi)\frac{\partial c_p}{\partial r}\right] - \Re_v(\xi) \qquad (1)$$

$$\frac{\partial \xi}{\partial t} = \frac{v_s}{1-\epsilon_0}\Re_v(\xi) \qquad (2)$$

The local conversion, ξ, is related to the porosity of the solid, ϵ_p, by the relation:

$$\xi = \frac{\epsilon_0 - \epsilon_p}{(1-\epsilon_0)(Z-1)} \qquad (3)$$

where ϵ_0 is the initial porosity, c_p is the concentration of SO_2 in the pores, ϵ_p^a is the accessible porosity of the solid, Z is the stoichiometric volume of reacted solid phase per unit volume of unreacted solid phase, and v_s is the volume of unreacted solid phase per mole of solid reactant.

Boundary conditions at the center and at the surface of the particles must be used to complete the differential equation resulting from the mass balance of the gaseous reactant. The usual no-flux ("symmetry") boundary condition is used at the center of the particle, while the boundary condition at the surface is obtained from a mass balance on the gaseous reactant there:

$$\left.\frac{\partial c_p}{\partial r}\right|_{r=0} = 0;\ D_e\left.\frac{\partial c_p}{\partial r}\right|_{r=a} = k_g(c_b - c_p)\Big|_{r=a} \qquad (4)$$

where a is the radius of the particles, k_g is the mass-transfer coefficient, and c_b is the concentration of the gaseous reactant in the bulk. The accessible porosity, ϵ_p^a, effective diffusion coefficient, D_e, and volume-based reaction rate, $\Re_v$, are assumed to be functions of the local conversion, and a structural model is needed to describe their variation with the progress of the reaction.

The assumption that the local structural properties of the solid are solely determined by the local conversion is valid only if the reaction obeys first-order kinetics or, for arbitrary kinetics, if the reaction rate at a point of the reaction surface is

independent of the radius of curvature. For first-order kinetics, the volumetric reaction rate can be expressed as:

$$\Re_v(\xi) = k_v(\xi) c_p \tag{5}$$

Introducing this expression in Eq. 1 and using the pseudo-steady-state approximation for the SO_2 concentration profile, it can be shown that the evolution of the concentration profiles with respect to a scaled time defined as:

$$\tilde{t} = \int_0^t \frac{c_b(t')}{c_b^*} dt' \tag{6}$$

with c_b^* being a reference concentration, should be independent of the concentration of sulfur dioxide in the bulk. Control experiments using samples of calcined solids and calcium oxide powders (Zarkanitis, 1991) showed that the differences between conversion vs. scaled time [defined for constant c_b as $\tilde{t} = (c_b/c_b^*)t$] curves for different ambient SO_2 concentrations, ranging from 3,000 to 500 ppm, were within the repeatability and reproducibility limits of the experiments. It was thus concluded that the reaction of the calcined sorbents with SO_2 had first-order, with respect to the concentration of SO_2, intrinsic kinetics in the temperature range covered by our experiments. The same conclusion was also reached, among others, by Marsh and Ulrichson (1985) for the sulfation of calcines derived from hydroxide precursors and Simons et al. (1987) for the sulfation of limestone calcines, but Borgwardt and Bruce (1986) concluded that the sulfation rate of the limestone calcines they studied depended nonlinearly on the partial pressure of SO_2 and determined a value of 0.62 for the exponent.

Structural model

The structural model used here to describe the evolution of the structure of the solid during the gas-solid reaction process is based on the mathematical model developed by Yu and Sotirchos (1987) for gas-solid reactions exhibiting pore closure behavior. This model considers a pore structure that can initially be represented by a network of finite in length cylindrical capillaries. After reaction starts, the pore (gas-solid interface) and reaction (reacted-unreacted solid interface) surfaces are represented by populations of overlapping cylinders coaxial to those forming the initial pore structure. As the conversion increases, pores close, and inaccessible pores or inaccessible clusters of pores form. For reaction times greater than zero, the pore network contains plugged pores, accessible pores, and inaccessible pores. The last kind of pores includes pores of finite radius that either terminate at sites of closed pores or belong to a finite cluster of open pores.

The initial pore structure is described by the length distribution density $l_0(R_0)$, with $l_0(R_0)dR_0$ being the length per unit volume of capillaries with size in the range $[R_0, R_0 + dR_0]$, with the initial pore-size range being $[R_{0*}, R_0^*]$. Percolation theory is used to follow the formation of inaccessible pores in the course of the reaction and the evolution of the distribution densities of plugged, accessible, and inaccessible pores. Equations for the rates of change of the radius of a pore that has evolved from a pore of initial radius R_0 at time t, $R_p(R_0,t)$, and of the radius of the corresponding capillary for the reaction surface, $R_r(R_0,t)$, are derived by solving the diffusion equation in the product layer with appropriate boundary conditions and writing a mass balance for the solid, respectively. In doing so, it is assumed that negligible reaction occurs at the reaction surface that belongs to capillaries coaxial to plugged or open, inaccessible pores. For more details on the structural model, the reader is advised to consult the article by Yu and Sotirchos (1987).

The volumetric reaction rate constant, k_v, is obtained by averaging the reaction rate at a point of the reaction surface, as it is predicted by the structural model, over the accessible reaction surface area (Yu and Sotirchos, 1987; Zarkanitis et al., 1990). The effective diffusivity may be determined by averaging the diffusion coefficient in a single capillary of radius R_p, $D(R_p)[=D_K(R_p)D_b/(D_K(R_p)+D_b)]$ over the accessible pore-size distribution, as it was done by Yu and Sotirchos (1987) in the first implementation of the generalized random pore model under conditions of intraparticle diffusional limitations. This approach, however, violates the mass balance equations at the nodes of a network of finite in length pores, since it assumes that microscopic and macroscopic concentration fields coincide (smooth field approximation).

For pore network structures, Burganos and Sotirchos (1987) proposed to determine the diffusion coefficient by applying the smooth field approximation (Jackson, 1977) to an equivalent, with respect to mass transport, network having uniform conductance (diffusivity × radius^2/pore length) for all pore segments. The equivalent network may be obtained by applying the effective medium theory to the original network. For uniform length pore segments, the EMT-SFA procedure leads to the following expression for the effective diffusivity:

$$D_e = \frac{\hat{\epsilon}_p}{3} \frac{\langle D(R_p) R_p^2 \rangle_e}{\langle R_p^2 \rangle_a} \tag{7}$$

where $\hat{\epsilon}_p$ is the porosity that the structure would have if *all* pores of initial size R_0 had size $R_p(R_0,t)$ at time t. $\langle \bullet \rangle_e$ represents the effective medium average of $\bullet$, obtained from the equation (Kirkpatrick, 1973):

$$\int_{R_0} \frac{\langle \bullet \rangle_e - \bullet}{\bullet + \left[\frac{1}{X_c} - 1\right] \langle \bullet \rangle_e} l_0(R_0) dR_0 = 0 \tag{8}$$

where X_c is the percolation threshold of the network, as it is predicted by the effective medium theory, which is equal to $2/z$ for networks built on regular lattices of coordination number z. Finally $\langle \bullet \rangle_a$ stands for the arithmetic average of $\bullet$ with weight function $l_0(R_0)$.

It is not necessary to solve the structural model equations simultaneously with Eqs. 1–4 since k_v and D_e depend only on ξ, and this dependence can be determined from the solution of the structural model. More details on the methods used to solve the equations for the diffusion and reaction model (Eqs. 1–4) and the structural model are given by Yu and Sotirchos (1987).

Estimation of Model Parameters

Accessibility of the network, pore-size distribution, and effective diffusivity

A Bethe lattice is used to represent the topology of the pore

network and determine its accessibility function, that is, the expression that provides the fraction of open, accessible pores in the network given the fraction of open pores. The accessibility function of Bethe lattices is given by an analytical expression which involves only its coordination number, z, as a parameter (Fisher and Essam, 1961). The use of a Bethe lattice does not limit the validity of the results obtained here since most two- and three-dimensional lattices have accessibility functions of similar shape. That is, given a different lattice, one can find a Bethe lattice (that is, a z) that will approximate its accessibility function sufficiently close.

Mercury porosimetry gives the void volume penetrated by mercury as a function of exerted pressure. If a structure of perfectly interconnected pores or infinitely long-pore segments is assumed, the pore-size distribution of the solid can readily be obtained from the porosimetry data (Washburn 1921; Drake, 1949). A rigorous application of the generalized pore model requires correction of the pore-size distribution that is extracted from mercury porosimetry data for a perfectly interconnected pore network or, equivalently, for a structure of infinitely long pores. This correction is needed because in a network of finite pore segments, a large pore is filled by mercury at a capillary pressure determined not by its own radius but by the radius of the feeder pore through which it is invaded by mercury. The correction of the pore-size distribution requires, among other things, the distribution of the length of the pores and the particle size of the sample used to obtain the mercury intrusion results or the use of an unknown parameter (Mishra and Sharma, 1988) that accounts for their effects on the mercury intrusion curve. The correction of the pore-size distributions obtained from mercury porosimetry data for pore network structures like those considered in this study was considered in detail by Zarkanitis (1991). The main difference between the uncorrected and corrected pore-size distributions (see also Mishra and Sharma, 1988) is that in the latter, part of the pore volume from the intermediate pore-size range is shifted to larger pore sizes. To avoid the introduction of additional parameters in the analysis of the experimental data, it was decided to employ the uncorrected pore-size distributions, that is, those obtained by assuming perfectly interconnected networks of pores (Figures 2-4). The consequences of this choice will be discussed during the presentation of our results.

The effective diffusivity can be computed using Eq. 7 with X_c set equal to $1/(z-1)$, that is, the percolation threshold of Bethe lattice structures. This approach was taken by Zarkanitis and Sotirchos (1989) in a preliminary analysis of limestone sulfation data. It was shown by Stinchcombe (1974) that a better approximation to the conductance of a Bethe lattice network away from the percolation threshold is obtained by using a larger value of X_c in the effective medium theory equation:

$$X_{ce} = 1 - 1/f(z);$$

$$f(z) = 1 + [1 + 1/(z-1)] \sum_{n=2}^{\infty} \frac{[1/(z-1)]^{n-1}}{1 + [1/(z-1)]^{2n-1}} \quad (9)$$

Equation 7 with X_c given by Eq. 9 was thus used for the computation of the effective diffusivity in the analysis of our experimental data. It should be noted that even though this approximation zeroes the effective diffusivity before the actual percolation threshold is reached, it does not make much difference which X_c value is used in Eq. 7, since $1/(z-1)$ and $1-1/f(z)$ are not much different and the effective conductance in the vicinity of the percolation threshold is very low.

Reaction rate constant and mass-transfer coefficient

For a first-order reaction with respect to the sulfur dioxide concentration and under isothermal conditions, the initial reaction rate per unit of particle volume is given by:

$$\overline{\mathcal{R}}_{v0} = (k_s c_b) S_0 \eta \quad (10)$$

with

$$\eta = \frac{3}{\Phi^2} \cdot \frac{\Phi \coth \Phi - 1}{1 + (\Phi \coth \Phi - 1)/Sh_e} \quad (11)$$

$$\Phi = a\sqrt{\frac{k_s S_0}{D_{e0}}}; \quad Sh_e = Sh\,\frac{D_b}{D_{e0}}; \quad Sh = \frac{k_g a}{D_b} \quad (12a\text{-}c)$$

The reaction rate constant k_s was estimated by minimizing the functional:

$$f = \sum_{i=1}^{4} (\overline{\mathcal{R}}^i_{\text{obs}} - \overline{\mathcal{R}}^i_{th})^2 \quad (13)$$

$\overline{\mathcal{R}}^i_{\text{obs}}$ is the experimentally observed initial reaction rate for particles of size i (1: 53-62, 2: 88-105, 3: 210-250, and 4: 297-350 μm), and $\overline{\mathcal{R}}^i_{th}$ is the reaction rate given by Eq. 10.

Using a correlation for the average mass-transfer coefficient at the surface of a sphere exposed to a flowing stream (Bird et al., 1960), the Sherwood number, Sh (see Eq. 12c), was found to be almost unity and practically independent of the particle size. Such a small value for the Sherwood number would imply strong external mass-transfer limitations for nonporous particles, but it is the effective Sherwood number, Sh_e (see Eq. 12b), that actually appears in the dimensionless form of the mathematical model. The value of Sh_e ranged from 30 to 250, depending on whether an infinite or finite value for the coordination number was employed. As a result, the external mass-transfer resistance had practically no effect on the predictions of the mathematical model: that is, the concentration at the surface of the particles was almost equal to that in the bulk of the gas phase. The difference between surface and bulk concentration was small even when the Sherwood number was taken to be an order of magnitude smaller than unity. This is a very important result, since because of the presence of the pan, the actual Sherwood number of the particles may be smaller than the value for stagnant diffusion around freely suspended spheres.

Z and v_s

The porous solids that result from calcination of limestones and dolomites contain calcium, magnesium oxide, and other inert species (see Table 1). Z is defined as the volume of reacted solid phase per unit of unreacted solid phase. Let Z_M, M = Ca or Mg, be the stoichiometric volume ratio when the pure oxide is converted to sulfate ($Z_M = v_{MSO_4}/v_{MO}$). When both oxides

Table 3. Z and v_s Values for Three Calcines*

Sample	Z	$v_s \times 10^3$ (m³/kmol)
Greer Limestone	3.037 (3.015)	17.32 (17.52)
Georgia Marble	3.022 (2.952)	17.43 (18.1)
Iceland Spar	3.078 (3.070)	16.97 (17.04)

*The values shown in parentheses are for MgO behaving as an inert species.

react with sulfur dioxide, a volume balance in the product layer gives (Yu, 1987):

$$Z = (Z_{Ca} - 1)\psi_{CaO} + (Z_{Mg} - 1)\psi_{MgO} + 1 \tag{14}$$

with ψ_i being the volume fraction of the species i in the solid phase. The definition of v_s as the volume of unreacted solid phase per mole of solid reactant leads to the expression:

$$\frac{1}{v_s} = \frac{\psi_{CaO}}{v_{CaO}} + \frac{\psi_{MgO}}{v_{MgO}} \tag{15}$$

with v_i being the molar volume of species i. When magnesium oxide is considered inert, Eqs. 14 and 15 become:

$$Z = (Z_{CaSO_4} - 1)\psi_{CaO} + 1 \tag{16}$$

and

$$v_s = \frac{v_{CaO}}{\psi_{CaO}} \tag{17}$$

The values of Z and v_s given by Eqs. 14 and 15 for the calcines examined in this study are shown in Table 3. The values shown in parentheses are those obtained when magnesium oxide is treated as an inert species (Eqs. 16 and 17). As it can be seen from Table 3, the values of Z are slightly lower if magnesium oxide is considered inert with respect to SO_2, while the v_s values are slightly higher. This is expected since the pure magnesium oxide has higher stoichiometric volume ratio but lower molar volume than calcium oxide, 4.01 vs. 3.09 and 11.04×10^{-3} m³/kmol vs. 16.9×10^{-3} m³/kmol, respectively.

Table 3 was constructed using 2.61 g/cm³ for the density of $CaSO_4$, a value taken from the *CRC Handbook of Chemistry and Physics* (Weast, 1988). In addition to the above value, a density of 2.96 g/cm³ is also listed in the same handbook for $CaSO_4$, and it is the only value appearing in *Perry's Handbook* (Perry, 1984). We chose to work with the smaller of the two values because it has been employed almost exclusively in past studies of limestone sulfation, and we wanted to make our results comparable with those reported there. Recent measurements by Gullett and Bruce (1989) indicated that the density of the solid product formed during sulfation of calcium oxide is equal to the larger of the two values given in the literature. Using a larger value for the density of $CaSO_4$ in the mathematical model used to analyze the experimental data would not affect in any way the conclusions reached in our study. However, it would lead to smaller Z values (2.725 instead of 3.09 for pure CaO) and, hence, higher ultimate conversions for complete pore plugging without formation of inaccessible pore space. As a result, smaller values of coordination number than those obtained for the Z values of Table 3 would have to be employed for all three solids to bring the model predictions into agreement with the experimental data.

Table 4. Coordination Number Reaction Rate Constant, and Product Layer Diffusivity Values Used in the Mathematical Model

Calcination/Sulfation Temperature (°C)	z	k_s (m/s)	D_p (m²/s)	k_s (m/s) for $z = \infty$
Greer Limestone				
850/700	12	2.39×10^{-5}	5.0×10^{-13}	2.01×10^{-5}
850/750	12	3.03×10^{-5}	9.0×10^{-13}	2.52×10^{-5}
850/850	12	3.29×10^{-5}	2.0×10^{-12}	2.74×10^{-5}
750/750	6	2.46×10^{-5}	9.0×10^{-13}	1.95×10^{-5}
Georgia Marble				
850/700	4	1.42×10^{-5}	9.0×10^{-14}	1.16×10^{-5}
850/750	4	1.83×10^{-5}	2.0×10^{-13}	1.47×10^{-5}
850/850	4	1.92×10^{-5}	2.0×10^{-12}	1.55×10^{-5}
750/750	3	1.34×10^{-5}	2.0×10^{-13}	1.15×10^{-5}
Iceland Spar				
850/700	6	1.31×10^{-5}	9.0×10^{-14}	1.02×10^{-5}
850/750	6	1.42×10^{-5}	2.0×10^{-13}	1.08×10^{-5}
850/850	6	1.73×10^{-5}	7.0×10^{-13}	1.28×10^{-5}
750/750	3	1.44×10^{-5}	2.0×10^{-13}	1.07×10^{-5}

Model Predictions and Experimental Results

The product layer diffusivity, D_P, and the network coordination number are the only parameters left to be determined for the application of the mathematical model to the experimental data obtained for the various calcines used in our experiments. For a given coordination number, we can calculate the initial effective diffusivity using the pore-size distribution of the solid and Eq. 7, and then use this value to estimate the reaction rate constant following the procedure outlined by Eqs. 10-13. According to the assumptions on which the random pore model was built, the coordination number should depend only on the characteristics of the pore structure of the solid. The product layer diffusivity, on the other hand, should depend on the microstructure of the reacted solid phase and the temperature at which diffusion takes place. These two parameters were thus determined by matching the model predictions with the experimental data under the constraints that the coordination number be the same for all particles of a given calcine and all sulfation temperatures provided that sulfation has been carried out at a temperature lower than the calcination temperature and that the diffusivity in the product layer vary only with the sulfation temperature and the limestone precursor.

The product layer diffusivity, coordination number, and reaction rate constant values that were determined at the various conditions used to carry out sulfation experiments in this study are shown in Table 4. The coordination numbers given in the table are for a Bethe lattice representation of the pore structure. A Bethe lattice with coordination number z is equivalent, with respect to the percolation threshold predicted by the effective medium theory ($X_c = 2/z$), to a regular lattice of coordination number $2(z-1)$. Thus, if a regular lattice representation is employed, the coordination numbers of 4 and 12 for Georgia marble and Greer limestone, respectively, at 850°C would become 6 and 22, respectively (Zarkanitis and

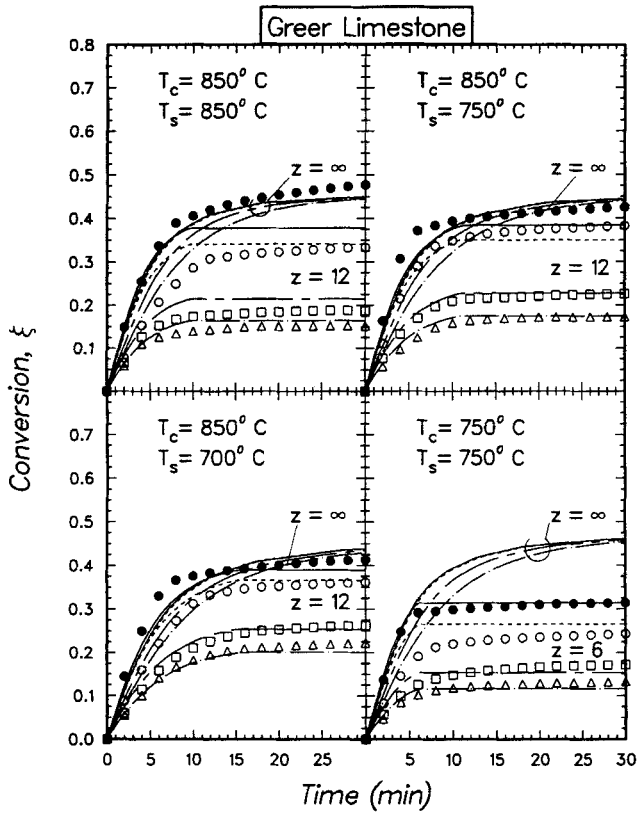

Figure 6. Experimental and theoretical conversion vs. time curves for Greer limestone calcines for various calcination temperatures, sulfation temperatures, and particle sizes.

●, —: 53-62 μm; ○, - - -: 88-105 μm; □, — - —: 210-250 μm; △, — · —: 297-350 μm. The model predictions are given by the continuous curves.

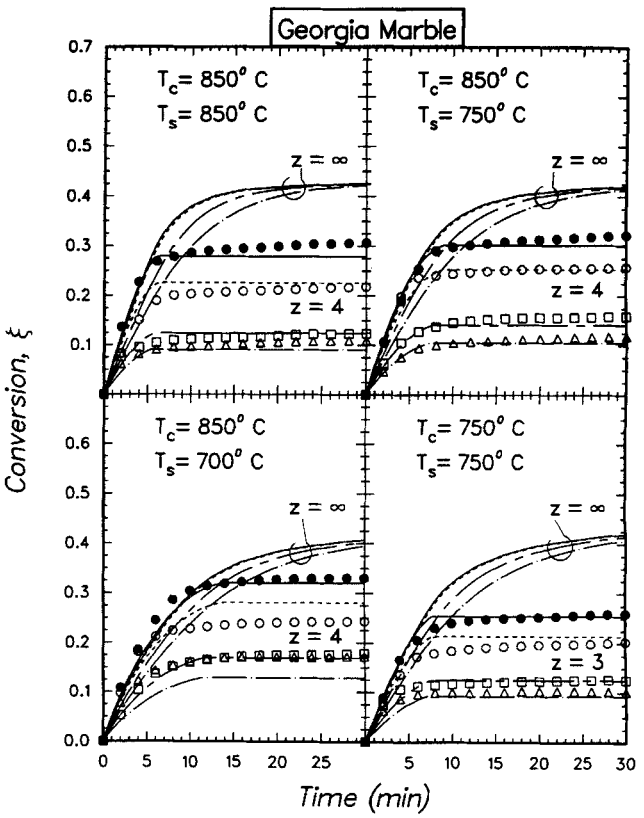

Figure 7. Experimental and theoretical conversion vs. time curves for Georgia marble calcines for various calcination temperatures, sulfation temperatures, and particle sizes.

●, —: 53-62 μm; ○, - - -: 88-105 μm; □, — - —: 210-250 μm; △, — · —: 297-350 μm. The model predictions are given by the continuous curves.

Sotirchos, 1989). Shown in Table 4 are also the kinetic constants that are obtained when the pores of the calcines are assumed to form a perfectly interconnected pore network ($z = \infty$). The rate constants for $z = \infty$ are smaller than those determined for finite coordination numbers because for a given pore-size distribution, the effective diffusivity increases with increasing coordination number.

The reaction trajectories predicted by the mathematical model for the sulfation of Greer limestone, Georgia marble, and Iceland spar calcines for the parameters of Table 4 are compared in Figures 6, 7 and 8, respectively, with the experimental conversion vs. time curves, the latter represented by distinct data points. The agreement between model predictions and experimental data should be deemed more than satisfactory considering the constraints under which the two free parameters, D_P and z, were estimated. The coordination number had to be the same for 12 different experiments (four particle sizes at three sulfation temperatures) for the calcines produced by calcination at 850°C and for four different experiments (four particle sizes sulfated at 750°C) for the calcines produced at 750°C. On the other hand, the solid product layer diffusivity had to be the same for all four particle sizes at each sulfation temperature regardless of calcination temperature.

The most noticeable differences between model results and experimental data are seen to occur for the small Greer limestone particles (53–62 μm). Forcing the model predictions to come into better agreement with the experimental data for these particles would lead to overestimation of the conversions reached by the larger particles. Similar behavior for the Greer limestone sample was also seen in its direct reaction with SO_2 under simulated pressurized fluidized-bed combustion conditions (Krishnan and Sotirchos, 1990) that prevent decomposition of calcium carbonate. Specifically, it was found that the conversions reached by the small Greer limestone particles were considerably larger than those that one would expect from a shrinking core model on the basis of the results for larger particles. These results suggest that small particles of calcined or uncalcined Greer limestone undergo some expansion during reaction with SO_2, yielding a more open structure that allows the reactant to reach the unreacted solid in the interior of the particles even after, in the case of the calcines, pore plugging takes place. Indeed, notice that after the point where the conversion tends to level off (about 10 min for most cases), the Greer limestone particles continue to react at a rate higher than other samples, with the 53–62 μm particles reaching at 850°C higher conversion than the value predicted for complete pore plugging of the pore space with solid product. Large deviations are also observed for the Iceland spar at 700°C, but for temperatures below 700°C, $CaSO_4$ is not the only product of the reaction of CaO with SO_2. Formation of $CaSO_3$ may take place,

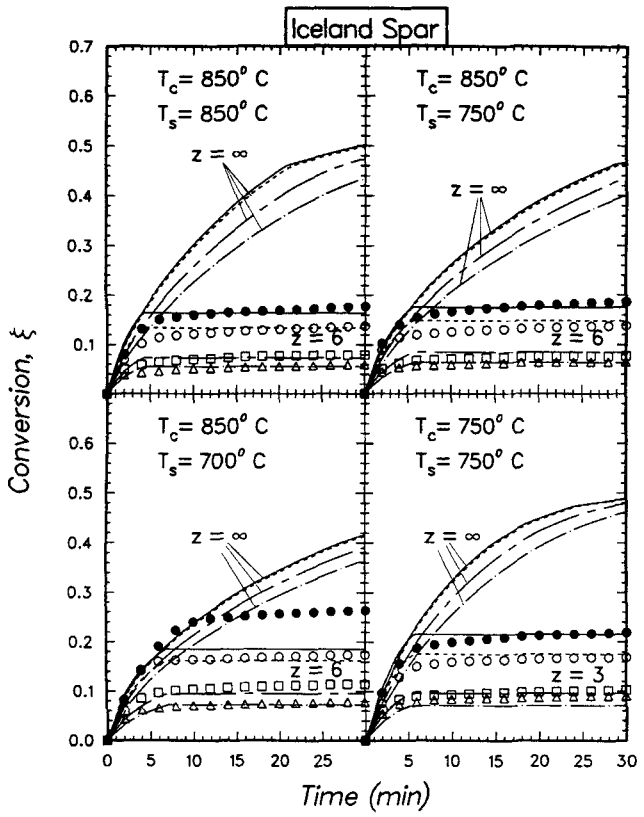

Figure 8. Experimental and theoretical conversion vs. time curves for Iceland spar calcines for various calcination temperatures, sulfation temperatures, and particle sizes.

●, —: 53-62 μm; ○, - - -: 88-105 μm; □, — - —: 210-250 μm; △, — · —: 297-350 μm. The model predictions are given by the continuous curves.

which causes pore plugging at higher conversions, since it occupies less space than $CaSO_4$. This is expected to have a stronger effect for the smaller particles since, as we will see later, our modeling results indicate that incomplete utilization of the capacity of small particles for SO_2 removal is due primarily to the formation of inaccessible (locally) pore space.

The reaction trajectories obtained from the mathematical model for a perfectly interconnected network of pores ($z = \infty$) are also shown in Figures 6-8. The product layer diffusivity used for $z = \infty$ was the same as that for the corresponding cases with finite coordination number, but qualitatively similar results were obtained for other D_P values. The results of Figures 6-8 for $z = \infty$ show that in this case the particle size influences the reaction trajectories only during the initial stages of the reaction. At larger reaction times, the trajectories for all particle sizes approach each other, reaching the same final conversion which corresponds to complete filling of the pore space of the porous calcines with solid product. For this reason, the quantitative differences between the model results for $z = \infty$ and the experimental data increase as the conversion reached by the solid in the experiment decreases. The largest differences occur for the Iceland spar calcines and the calcines of the other two samples that were produced by calcination at 750°C. The agreement between the model results for $z = \infty$ and the experimental data can be improved only by using effective diffusion coefficients in the intraparticle space much smaller than those predicted by Eq. 7 for $z = \infty$, specifically a conversion-dependent tortuosity factor. Such a choice, however, will not agree with the assumptions on which the development of the mathematical model for perfectly interconnected pores is based.

Calcination at 750°C produced calcines with lower sorptive capacity for SO_2 removal, for all particle sizes, than the samples obtained by calcining the same precursors at 850°C. The sorptive capacity of the three samples increased for each combination of particle size, calcination temperature, and sulfation temperature used in our study in the order Iceland spar → Georgia marble → Greer limestone. The coordination number that was determined by fitting the model predictions to the experimental data decreased, in general, with decreasing sorptive capacity; it decreased with decreasing calcination temperature and in the directions Greer limestone → Georgia marble and Greer limestone → Iceland spar. As it was pointed out in the description of the structural model, the coordination number is a measure of the extent of pore interaction (interlinking) in the interior of the porous medium: the larger its value, the higher the interaction of pores of different size. Therefore, calcination at a lower temperature appears not only to shift the apparent pore-size distribution of the calcined solids toward smaller pore sizes (see Figures 2-4), but to decrease the extent of pore interlinking in the structure as well. Moreover, the prediction of decreasing coordination number with decreasing sorptive capacity points to the conclusion that the connectivity of the pore structure is among the factors that have the most influence on ultimate sorbent utilization under given operating conditions.

The relative behavior of the reactivity evolution results for the Georgia marble and Iceland spar calcines is in apparent disagreement with the above conclusions and observations. The coordination number of the Iceland spar calcine is not smaller than that of Georgia marble sample for the same calcination temperature even though its capacity for SO_2 removal is lower at all reaction conditions (see Figures 9 and 10). The extents of pore interaction and communication in the interior of different porous media, however, can safely be compared in terms

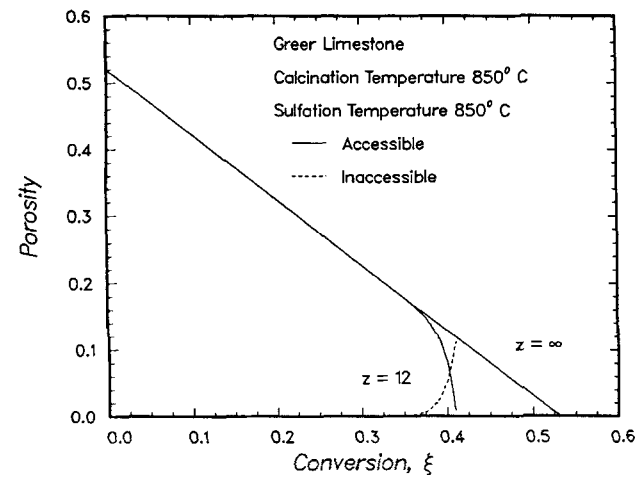

Figure 9. Variation of the accessible and inaccessible porosity of Greer limestone with the conversion at 850°C (calcination and sulfation) given by the mathematical model.

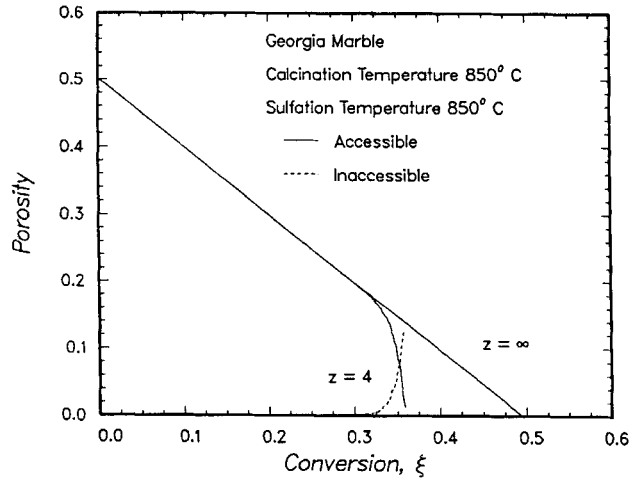

Figure 10. Variation of the accessible and inaccessible porosity of Georgia marble with the conversion at 850°C (calcination and sulfation) given by the mathematical model.

of the coordination numbers only for the same pore-size distribution. The pore-size distribution of the Iceland spar sample differs qualitatively from that of other samples for both calcination temperatures. It is practically bimodal having a significant fraction of pore volume that belongs to pores with the size smaller than the lower bounds of the pore-size ranges of the other two solids (see Figures 2–4). This situation is more pronounced for the solid produced by calcination at 850°C. Since all pores are assumed to participate in the same way in the pore network, the small pores account for a disproportionately large fraction of the total number of pores in the structure. (For independently distributed pore length and size, the number distribution density or equivalently length distribution density can roughly be approximated by dividing the porosity distribution density by the square of the pore radius.) Small pores are plugged with solid product at very low conversions; as a result, the model would predict that the pore structure of the Iceland spar samples becomes inaccessible to SO_2 at very low conversions if coordination numbers smaller than those of the Georgia marble sample were employed, especially for calcination at 850°C.

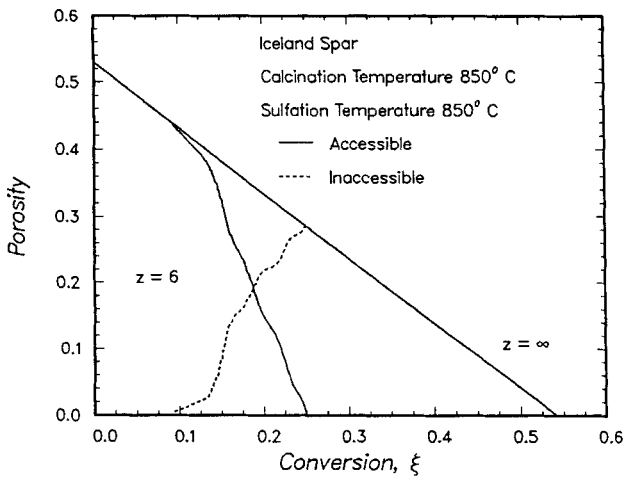

Figure 11. Model-predicted variation of the accessible and inaccessible porosity of Iceland spar with the conversion at 850°C (calcination and sulfation).

A more informative picture of the relation between the accessibility of the internal structure of a calcine and its capacity for SO_2 removal is obtained by plotting the variation of the accessible porosity of the reacting solid with the total porosity, as it is predicted by the mathematical model. Such plots are presented in Figures 9–11 for the three solids used in this study for calcination and sulfation at 850°C. Similar results are obtained for other combinations of calcination and sulfation temperatures. The pore size at which percolation takes place, that is, the structure becomes inaccessible, is independent of the sulfation temperature: it depends only on the pore-size distribution and can be found for a continuous pore-size distribution as the pore size R_{0c} that satisfies the equation:

$$\frac{\int_{R_{0*}}^{R_{0c}} l_0(R_0)dR_0}{\int_{R_{0*}}^{R_0^*} l_0(R_0)dR_0} = X_c \tag{18}$$

where X_c is the number fraction-based percolation threshold of the solid [$= 1/(z-1)$ for Bethe-lattice structures]. The conversion or, equivalently, total porosity that the solid has when the pore space becomes inaccessible is influenced, though weakly, by the sulfation temperature because of its effect on the relative rates of shrinkage of pores of different size. As the comparison of Figures 10 and 11 shows, the model predicts that the Iceland spar sample has the highest percolation threshold in terms of the porosity—the lowest in terms of conversion—even though it has higher coordination number and smaller number fraction-based percolation threshold (at 850°C) than the Georgia marble calcine. Its accessible porosity becomes zero at 25% conversion, while the corresponding values for the Greer limestone and Georgia marble samples are 41% and 36%, respectively. These conversion levels are those that would be obtained if the reaction occurred under conditions controlled by kinetics and diffusion in the product layer. Of course, if no accessible pore volume formation took place, the ultimate conversions reached in the absence of significant concentration gradients in the pore space would be equal to $\epsilon_0/[(1-\epsilon_0)(Z-1)]$ (about 50% for each case). It should be pointed out that while the coordination number needed to reproduce the experimental data is influenced strongly by the pore-size distribution, the porosity- or conversion-based percolation threshold is influenced weakly by it. This is a very important observation since, as mentioned before, the pore-size distribution obtained from mercury porosimetry data may have to be corrected for a rigorous application of the generalized pore model.

The variation of the effective diffusivity with the conversion for calcination and sulfation at 850°C, predicted by the mathematical model, is shown in Figure 12 for all three solids. It is seen that the intraparticle diffusion coefficient for a finite coordination number not only is initially much lower than that for thoroughly interlinked pores ($z = \infty$), but also decreases relatively faster as small pores close and formation of inac-

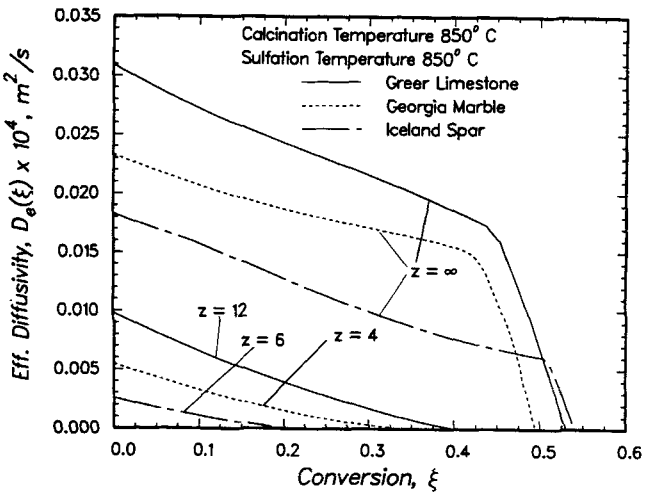

Figure 12. Model-predicted variation of the effective diffusivity with the conversion for the three solids at 850°C (calcination and sulfation).

cessible pore space takes place. It is because of the low resistance for intraparticle mass transport for $z = \infty$ that complete pore plugging at the external surface does not occur and the predicted conversion trajectories for all particle sizes eventually approach each other. The Iceland spar sample has the lowest diffusivity for perfectly interlinked pores ($z = \infty$) even though the middle part of its pore-size distribution is shifted toward larger pore sizes relative to that of the Georgia marble sample (see Figures 3 and 4). The main cause for this behavior is the presence of a smaller fraction of large pores in the Iceland spar samples. The effective diffusivities for $z = \infty$ increase in the order Iceland spar → Georgia marble → Greer limestone, that is, in the same order as the percolation thresholds (in terms of conversion, see Figures 9-11). As a result, the same order of diffusivity variation prevails for finite coordination numbers. Since the effective diffusivity is computed using the effective threshold, X_{ce} (Eq. 9), in Eq. 8, the effective diffusivity becomes zero and the interior of the porous solid inaccessible at a higher number fraction of open pores than the actual (number fraction-based) percolation threshold of the Bethe lattice structure $[1/(z-1)]$. For instance, the number fraction-based percolation threshold of the Georgia marble sample of Figure 10 is 0.333 ($z = 4$), but the effective value used in Eq. 8 equals 0.393. Nevertheless, in the vicinity of the percolation threshold, the effective diffusivity predicted by Eq. 7 for $X_c = 1/(z-1)$ has very low values; therefore, under significant intraparticle limitations—as it is usually the case—using $X_c = 1/(z-1)$ or $X_c = X_{ce}$ in Eq. 8 has no appreciable effects on the model predictions.

The evolution of the accessible pore-size distribution of the Iceland spar sample during sulfation at 850°C following calcination at the same temperature, as it is predicted by the mathematical model, is shown in Figure 13. The evolution of the pore-size distributions of the other two solids is similar, but the weakly bimodal form of the initial pore-size distribution of the Iceland spar sample makes its evolution slightly more interesting. The small pores of the structure become plugged with solid product at very low conversion (high porosity); thus, the accessible pore-size distribution of the Iceland spar calcine for the two nonzero conversion levels shown in the figure is unimodal. To validate the results of Figure 13 experimentally, we must produce partially reacted samples with uniform conversion profile in their interior. Otherwise, the obtained pore structure characterization (mercury porosimetry or gas adsorption) data will be representative of the average pore-size distribution of the partially reacted particles. Because of the very low diffusivity of SO_2 in the intraparticle space, significant concentration and conversion gradients are present even in the 53-62 μm particles (see Figure 14), and one may have to go to micron-size particles to eliminate the effects of intraparticle diffusion. It should be kept in mind though that the assumptions on which the development of the mathematical model used to obtain the results of Figure 13 and of the other figures of this study is based—such as negligible contribution of the external surface in the reaction process and pore length much smaller than the average particle size—may not be valid for very small particles.

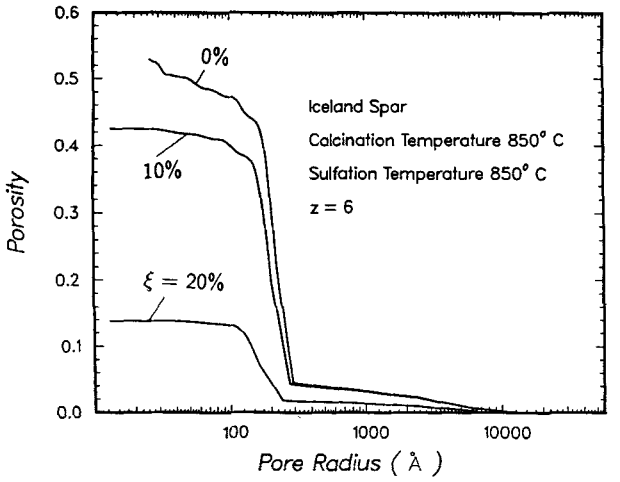

Figure 13. Model-predicted variation of the accessible pore-size distribution of Iceland spar with the conversion at 850°C (calcination and sulfation).

Figure 14 shows the sulfur dioxide concentration, solid conversion, and local porosity profiles predicted by the mathematical model for the Georgia marble sample calcined and sulfated at 850°C for two different particle sizes at two particle conversion levels: 10% and 29% for particles in the size range 53-62 μm and 5% and 9% for the 297-350 μm. The 53-62-μm particles exhibit lower diffusional limitations at the early stages of the sulfation reaction than larger particles; thus, the concentration and the solid conversion gradients are much larger for the latter. As the sulfation reaction progresses, the increasing solid conversion in the vicinity of the external surface of the particles leads to higher diffusion resistance there, which in turn gives rise to steeper sulfur dioxide concentration profiles. Although the small-size particles react under negligible intraparticle diffusional limitations at the onset of the sulfation reaction, intraparticle diffusion gains importance at higher conversions and eventually dominates the process. When the porosity at the external surface of the particles becomes (see Figure 12) 14.5%, the open space in their interior becomes inaccessible and reaction ceases. There are still open pores

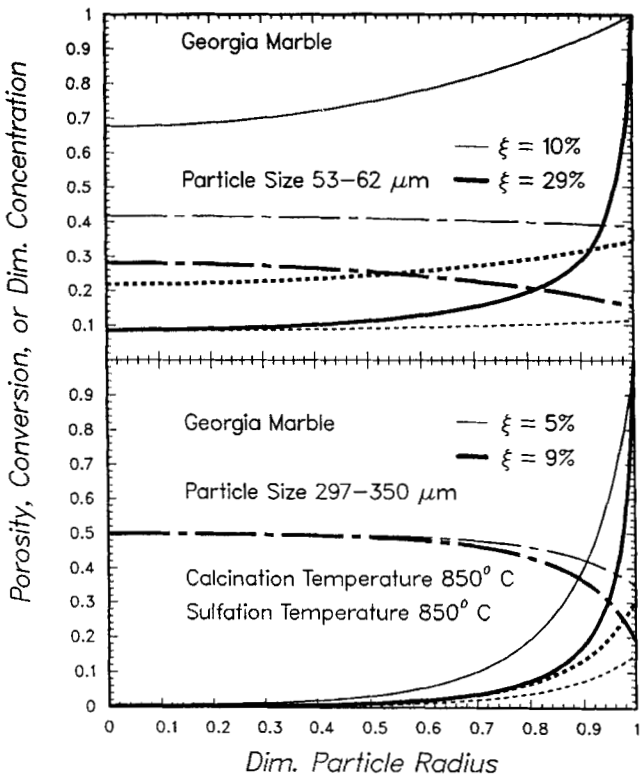

Figure 14. Model-predicted porosity, conversion, and SO_2 concentration profiles in the interior of Georgia marble particles.

—: concentration; - - -: conversion; - — -: porosity.

emanating from the external surface—since the total porosity is not zero—but the void space in the particle is not accessible because all these pores belong to finite clusters. The conversion at the center of small particles is not much different from that at their surface when pore closure takes place; as a result, their sorptive capacity is limited primarily by the formation of inaccessible pore space. On the other hand, the conversions

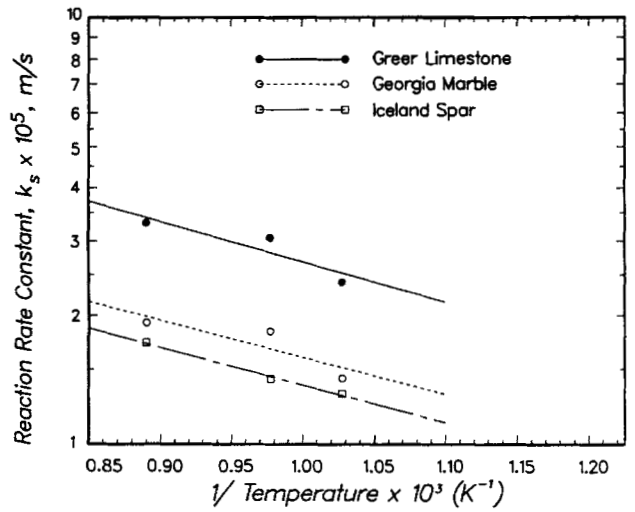

Figure 15. Arrhenius-type plots for the kinetic constants.

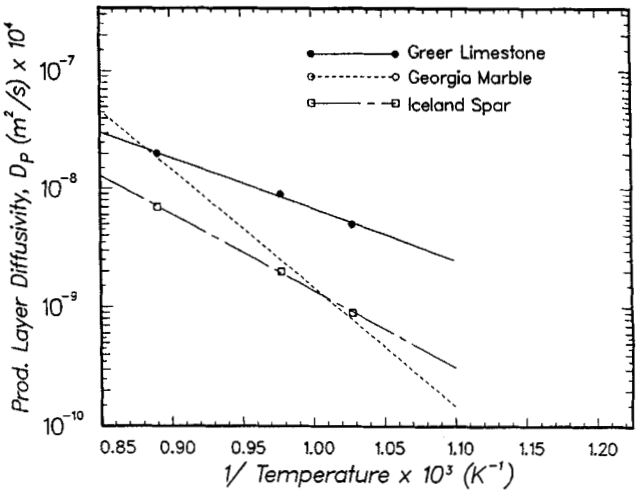

Figure 16. Arrhenius-type plots for the product layer diffusivities.

reached by large particles are also influenced by intraparticle diffusional limitations since only a thin crust in the vicinity of the external surface of large particles participates in the sulfation reaction.

Figures 15 and 16 present Arrhenius-type plots of the intrinsic reaction rate constant k_s and the product layer diffusivity D_P, respectively, for the sulfation reaction of the limestones used in this study. There is little variation of the activation energy of reaction among the three samples—it has an average value of about 17 kJ/mol—but the activation energy for diffusion in the product layer covers the rather broad range of 80–190 kJ/mol. A wide range of values for the activation energy of the CaO-SO_2 reaction has been reported in the literature. For example, Borgwardt (1970) reported activation energies for the sulfation reaction in the range 34–76 kJ/mol for several limestones in the temperature range 540–1,100°C, Doğu (1981) found an activation energy of about 50 kJ/mol in the temperature range 750–940°C, and Stouffer and Yoon (1989) reported an average activation energy of 153 kJ/mol in the range 800–1,000°C. The reported activation energies for product layer diffusion, on the other hand, lie in a less wide range: for example, 142 kJ/mol (Hartman and Trnka, 1980); 120 kJ/mol (Bhatia and Perlmutter, 1981); 102 kJ/mol (Christman and Edgar, 1983); 149 kJ/mol (Marsh and Urichson, 1985); and 138 kJ/mol (Borgwardt et al., 1987).

When comparing activation energies for the CaO-SO_2 reported by different investigators, it should be kept in mind that these numbers depend strongly on the experimental arrangement used to carry out the reaction, the method used for the analysis of the experimental data and the accuracy by which the initial reaction rate data have been measured. The reaction rate constant usually influences only the initial stages of the evolution of the reactivity of the solid, since once a relatively thick layer of product is formed, the local rate of reaction is controlled by diffusion in the product layer, because of the high resistance for diffusion in the product layer. As we mentioned during the description of experimental procedures and test experiments, many difficulties are involved in obtaining initial reactivity data free of interparticle mass transfer and sample size effects. Moreover, although the initial reaction rate is influenced in general by the resistance for intraparticle

diffusion (see Figure 14), in a number of studies the reported kinetic constants were based on the observed reaction rates without correction for intraparticle diffusion. Analogous observations apply to the activation energies for diffusion in the product layer.

Summary and Remarks

A detailed analysis of a set of experimental conversion vs. time data for the sulfation of calcines derived from three stones of high (>95%) calcium carbonate content was presented in this study. The analysis of the experimental data placed emphasis on the formation of inaccessible pore space and its effects on limiting the capacity of calcined limestones below the levels that are predicted by the stoichiometry of the reaction for complete pore plugging. This was accomplished by analyzing the experimental data using a detailed model for transport, reaction, and structure evolution in gas-solid reactions with solid product (Yu and Sotirchos, 1987), such as the reaction of calcined limestones with sulfur dioxide in the presence of oxygen. A network of pores consisting of cylindrical pore segments arranged on a Bethe lattice, a tree-like structure, was used to represent the pore structure of the calcined solids. The coordination number of the pore network and the diffusivity in the product layer were used as free parameters in matching the model predictions with the experimental data, with all other parameters determined from independent measurements. To assess both the correlative and predictive capabilities of the diffusion, reaction and structure evolution model, the experimental data used in our analysis covered relatively broad ranges of particle size, calcination temperature and sulfation temperature.

The predictions of the mathematical model were in very good agreement with the experimental data over the whole parameter range covered in our experiments. The connectivity of the pores in the structure, quantified by the coordination number for a given pore-size distribution, was found to play a major role in determining the capacity of calcines for SO_2 removal. The smaller the coordination number, the higher the fraction of porosity that exists in the form of finite pore clusters when the interior of the solid becomes inaccessible to diffusion. Inaccessible pore volume formation is the main reason for the observed low capacities of small particles for SO_2 removal. Large particles, on the other hand, are influenced both by inaccessible pore volume formation and intraparticle mass-transport limitations (that is, nonuniform conversion profiles in the interior).

The most interesting finding of our study is that the sorptive capacity and reactivity of calcines derived from the three samples increased for each calcination temperature in the direction of decreasing grain size in the rock precursors. This finding is in qualitative agreement with a similar result by Hartman and Pata (1979), who reported that calcines from coarse-grain precursors gave lower ultimate conversions than those derived from fine-grain stones. The reactivity evolution data that were obtained in our study during calcination of the precursors also gave increasing rate of calcination with decreasing grain size, indicating that limestones with fine grains yield calcines with pore structure of lower diffusional resistance. These results point to the conclusion that the petrographic texture of the precursor plays a major role in determining the pore-size distribution of the solid and the topological features (such as pore connectivity) of the pore structure of the resulting calcine. The decreasing pore connectivity with increasing grain size may be explained by considering the mechanism of calcination of calcium carbonate solids. Solid decomposition most probably starts at the periphery of the crystallites, at the grain boundaries. In a solid matrix of coarse grains, each particle is essentially part of a single grain, and therefore, the produced CO_2 is transported to the surface of the particles primarily through the porous oxide layer that surrounds the unreacted core of the grains. In particles obtained from solids of fine grains, on the other hand, CO_2 can also escape through the intercrystallite space. In both cases, pores are formed because of shrinkage of the solid phase during decomposition. However, if the pores formed at the grain boundaries of the original solid are larger than those formed in the interior of the grains, one would expect the pore structures of calcines obtained from fine-grain precursors to comprise an extensive network of highly interconnected large pores.

Acknowledgment

This research was supported by a grant from the U.S. Department of Energy. The stipend of S.Z. was covered partially by a fellowship from the Link Foundation. The pore structure of the solids was characterized using equipment acquired through an NSF equipment grant.

Notation

a = radius of the particle
c_p = concentration of SO_2 in the pores
c_b = concentration of SO_2 in the bulk of the gas phase
D_b = bulk diffusion coefficient of SO_2
D_e = effective diffusion coefficient of SO_2
D_P = diffusion coefficient in the product layer
$D_K(R)$ = Knudsen diffusion coefficient of SO_2 in a capillary of radius R
k_g = mass-transfer coefficient
k_s = intrinsic reaction rate constant (m/s)
$l_0(R_0)dR_0$ = length per unit volume of pores with size in the range $[R_0, R_0+dR_0]$
r = radial distance in a particle
R = capillary radius
R_0 = pore size at $t=0$
R_{0*} = lower limit of pore size range
R_0^* = upper limit of pore size range
$R_p(R_0,t)$ = size of a pore of initial size R_0 at the pore surface at time t
$R_r(R_0,t)$ = size of a pore of initial size R_0 at the reaction surface at time t
$\mathcal{R}_s$ = intrinsic reaction rate, per unit of reaction surface area
$\mathcal{R}_v$ = volumetric reaction rate, per unit of particle volume
S_0 = initial internal surface area
Sh = Sherwood number (see Eq. 12c)
Sh_e = effective Sherwood number (see Eq. 12b)
t = time
v_i = specific molar volume of solid i
X_c = number fraction-based percolation threshold
z = coordination number of the pore network
Z = stoichiometric volume ratio (volume of reacted solid phase per unit volume of unreacted solid phase)

Greek letters

ϵ_p = porosity
ϵ_p^a = accessible porosity
ϵ_0 = initial porosity
η = effectiveness factor
ξ = solid conversion
$\bar{\xi}$ = average conversion $[=\int_0^1 \xi d(r/a)^3]$
Φ = Thiele modulus
ψ_i = volume fraction of solid i in the solid phase

Literature Cited

Bhatia, S. K., and D. D. Perlmutter, "The Effect of Pore Structure on Fluid-Solid Reactions: Application to the SO_2-Lime Reaction," *AIChE J.*, **27**, 226 (1981).

Bird, R. B., W. E. Stewart, and E. N. Lightfoot, *Transport Phenomena*, Wiley, New York (1960).

Borgwardt, R. H., "Kinetics of the Reaction of SO_2 with Calcined Limestone," *Environ. Sci. Technol.*, **4**, 59 (1970).

Borgwardt, R. H., and K. R. Bruce, "Effect of Specific Surface Area on the Reactivity of CaO with SO_2," *AIChE J.*, **32**, 239 (1986).

Borgwardt, R. H., K. R. Bruce, and J. Blake, "An Investigation of Product-Layer Diffusivity for CaO Sulfation," *Ind. Eng. Chem. Res.*, **26**, 1993 (1987).

Borgwardt, R. H., W. F. Roache, and K. R. Bruce, "Method for Variation of Grain Size in Studies of Gas-Solid Reactions," *Ind. Eng. Chem. Fundam.*, **25**, 165 (1986).

Burganos, V. N., and S. V. Sotirchos, "Diffusion in Pore Networks: Effective Medium Theory and Smooth Field Approximation," *AIChE J.*, **33**, 1678 (1987).

Chan, R. K., K. S. Murthi, and D. Harrison, "Thermogravimetric Analysis of Ontario Limestones and Dolomites: II. Reactivity of Sulfur Dioxide with Calcined Samples," *Can. J. Chem.*, **48**, 2979 (1970).

Christman, P. G., and T. F. Edgar, "Distributed Pore-Size Model for Sulfation of Limestone," *AIChE J.*, **29**, 388 (1983).

Crowley, J. A., "A Reaction/Adsorption System for Gas-Solid Reaction Studies," MS Thesis, Univ. of Rochester (1985).

Drake, L. C., "Pore Size Distribution in Porous Materials: Application of High Pressure Mercury Porosimeter to Cracking Catalysts," *Ind. Eng. Chem.*, **41**, 780 (1949).

Dogu, T., "The Importance of Pore Structure and Diffusion in the Kinetics of Gas-Solid Noncatalytic Reactions: Reaction of Calcined Limestone with SO_2," *Chem. Eng. J.*, **21**, 213 (1981).

Fisher, M. E., and J. W. Essam, "Some Cluster Size and Percolation Problems," *J. Math. Phys.*, **2**, 609 (1961).

Gregg, S. J., and K. S. W. Sing, *Adsorption, Surface Area, and Porosity*, Academic Press, New York (1982).

Gullett, B. K., and K. R. Bruce, "Pore Distribution Changes of Calcium-Based Sorbents Reacting with Sulfur Dioxide," *AIChE J.*, **33**, 1719 (1987).

Gullett, B. K., and K. R. Bruce, "Identification of $CaSO_4$ Formed by Reaction of CaO and SO_2," *AIChE J.*, **35**, 1739 (1989).

Hartman, M., and R. W. Coughlin, "Reaction of Sulfur Dioxide with Limestone and the Influence of Pore Structure," *Ind. Eng. Chem. Process Des. Dev.*, **13**, 248 (1974).

Hartman, M., and J. Pata, "Texture of a Limestone Calcine and Its Reactivity with Sulphur Dioxide," *Coll. Czech. Chem. Comm.*, **44**, 2465 (1979).

Hartman, M., and O. Trnka, "Influence of Temperature on the Reactivity of Limestone Particles with Sulfur Dioxide," *Chem. Eng. Sci.*, **35**, 1189 (1980).

Jackson, R., *Transport in Porous Catalysts*, Elsevier, Amsterdam (1977).

Kirkpatrick, S., "Percolation and Conduction," *Rev. Modern Phys.*, **45**, 574 (1973).

Krishnan, S. V., and S. V. Sotirchos, "On the Mechanism of the Direct Reaction of Limestones with SO_2," AIChE Meeting, Chicago (1990).

Marsh, D. W., and D. L. Ulrichson, "Rate and Diffusional Study of the Reaction of Calcium Oxide with Sulfur Dioxide," *Chem. Eng. Sci.*, **40**, 423 (1985).

Mishra, B. K., and M. M. Sharma, "Measurement of Pore Size Distributions from Capillary Pressure Curves," *AIChE J.*, **34**, 684 (1988).

Perry, R. H., ed., *Chemical Engineers' Handbook*, 6th ed., McGraw-Hill, New York (1984).

Schroeter, L. C., *Sulfur Dioxide—Application in Foods, Beverages, and Pharmaceuticals*, Pergamon Press, London (1966).

Simons, G. A., A. R. Garman, and A. A. Boni, "The Kinetic Rate of SO_2 Sorption by CaO," *AIChE J.*, **33**, 211 (1987).

Sotirchos, S. V., J. A. Crowley, and H. C. Yu, "A Reaction/Adsorption Device for Gas-Solid Reaction Studies," *Chem. Eng. Commun.*, **71**, 83 (1988).

Stinchcombe, R. B., "Conductivity and Spin-Wave Stiffness in Disordered Systems—an Exactly Soluble Model," *J. Phys. C: Solid State Phys.*, **7**, 179 (1974).

Stouffer, M. R., and H. Yoon, "An Investigation of CaO Sulfation Mechanisms in Boiler Sorbent Injection," *AIChE J.*, **35**, 1253 (1989).

Washburn, E. W., "Note on a Method of Determining the Distribution of Pore Sizes in a Porous Material," *J. Phys.*, **7**, 115 (1921).

Weast, R. H., ed., *CRC Handbook of Chemistry and Physics*, CRC Press, Boca Raton, FL (1988).

Yu, H. C., "Theoretical and Experimental Studies on Gas-Solid Reactions with Solid Product," PhD Thesis, Univ. of Rochester (1987).

Yu, H. C., and S. V. Sotirchos, "A Generalized Pore Model for Gas-Solid Reactions Exhibiting Pore Closure," *AIChE J.*, **33**, 382 (1987).

Zarkanitis, S., "Pore Structure and Reactivity Evolution during Limestone Sulfation," PhD Thesis, Univ. of Rochester (1991).

Zarkanitis, S., E. A. Efthimiadis, and S. V. Sotirchos, "Experimental Evaluation of a Class of Distributed Pore Size Models for Gas-Solid Reactions with Solid Product," *Chem. Eng. Sci.*, **45**, 2761 (1990).

Zarkanitis, S., and S. V. Sotirchos, "Pore Structure and Particle Size Effects of Limestone Capacity for SO_2 Removal," *AIChE J.*, **35**, 821 (1989).

Manuscript received Dec. 16, 1991, and revision received May 18, 1992.